

The Comparison of Fragility Curves of Moment-Resisting and Braced Frames Used In Steel Structures under Varying Wind Load

Abdulkadir OZALP^{1*}
Hande GOKDEMIR²
Cihan CIFTCI³



ABSTRACT

In this study, the performance of two different steel structure types (moment-resisting frame and braced frame) under wind loading was compared by addressing the fragility curves of these structure types. To perform this comparison, the dimensions of the members of these structural systems were first determined. Then, nonlinear static pushover analyses were conducted to assess the performance levels of each frame type. After applying these analyses, time-history analyses were performed with 100 different wind loads for each varying equivalent mean wind speed. Afterwards, the probability of exceeding the predetermined structural performance limits of the structure types was determined using Monte Carlo simulation method. Finally, the results of the simulation method were used to adapt the maximum likelihood estimation method to obtain the fragility curves of the structures. To conclude, it has been revealed that the material cost of the structure doubles when diagonal elements are used, but the wind speed required for a 100% collapse probability to occur in the braced frame is twice as high compared to the moment-resisting frame.

Keywords: Performance based design, time history analysis, pushover analysis, load resistance factor design, fragility curve.

Note:

- This paper was received on November 29, 2022 and accepted for publication by the Editorial Board on July 27, 2024.
- Discussions on this paper will be accepted by May 31, 2025.
- <https://doi.org/10.18400/tjce.1211905>

1 Presidency of the Republic of Türkiye Directorate of Communications, Ankara, Türkiye
abdulkadir.ozalp@iletisim.gov.tr - <https://orcid.org/0000-0002-8951-6841>

2 Eskişehir Osmangazi University, Department of Civil Engineering, Eskişehir, Türkiye
handeg@ogu.edu.tr - <https://orcid.org/0000-0003-0478-8133>

3 Abdullah Gül University, Department of Civil Engineering, Kayseri, Türkiye
cihan.ciftci@agu.edu.tr - <https://orcid.org/0000-0001-9199-6437>

* Corresponding author

1. INTRODUCTION

Thanks to the advancing technology and production techniques, many different structures can be built today. In order to make these structures sustainable, the analysis and design of the structures are important. In the application of these analyses and designs, not only the stiffness values of the structures but also the external loads acting on the structures have an extremely important role. Among these external loads, hurricanes are one of the most destructive natural disasters that can cause serious damage to structures and loss of life due to the wind forces that they exert (especially for high-rise buildings to be the subject of this study). Meanwhile, this destructive effect of wind loads is also directly related to the geographical region where the structure is located. Since the size and distribution of wind loads vary according to geographical regions in the world, for example, according to the World Wind Map [1] given in Fig. 1, the wind speed is quite high on the east coast of the United States.

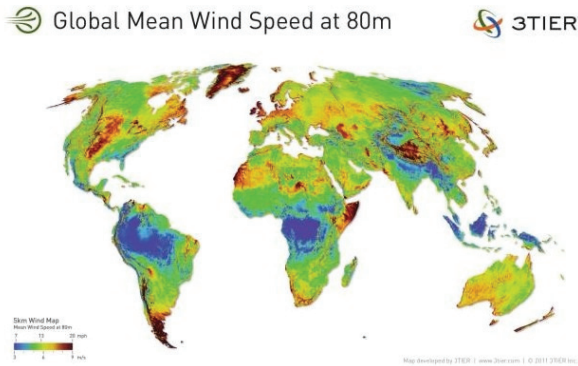


Figure 1 - The distribution of the average wind speed at 80 m height in the world

Hurricanes are common on the east coast of the US. In Fig. 2, wind speeds of office buildings located on the southeast and east coasts of USA are given [2]. According to the structural design regulations, these wind speeds are taken into account in the design calculations of buildings. However, in some cases, wind speeds can exceed these values, especially in hurricanes. The reason why such situations are ignored in regulations is that wind-caused natural events are not seen very often. However, in such situations, the effect of wind loads can be much more destructive. For example, Hurricane Sandy caused about \$65 billion cost in property damage in the Ontario province of Canada and the northeastern coast of the United States [3]. Due to the severity, intensity, and effects of hurricanes in America, this country is chosen as the geography in this study.

Risk represents the probability of occurrence of hazardous events and the function of their social and economic impact. The search for more efficient methods to reduce risks and quantify these risks has led to the development of performance-based engineering approach. Performance-based engineering covers a wide place in the literature [4]. The main philosophy of the performance-based design is based on the material properties, type and dimensions of the selected building member to provide the targeted performance for the predetermined hazard level [5].

As mentioned above, in extraordinary situations such as natural disasters, the safety of buildings designed according to specific standards cannot be ensured [6]. If the force-displacement graph of the performance levels of the structures is known, it can be predicted when the structure will need to be evacuated, whether it can be used or not and when it will collapse. Then, performance-based analysis of buildings is of great importance in order to reduce the loss of life and property that may occur [7]. The fragility curves developed as a result of the performance-based analysis to predict the probability of collapse of the structures under varying wind speeds.

Fragility curves are cumulative distribution functions that enable to obtain the variability in the increment of probability of reaching damage states including engineering parameters such as story drift or exceeding these damage threshold limits [8–10].

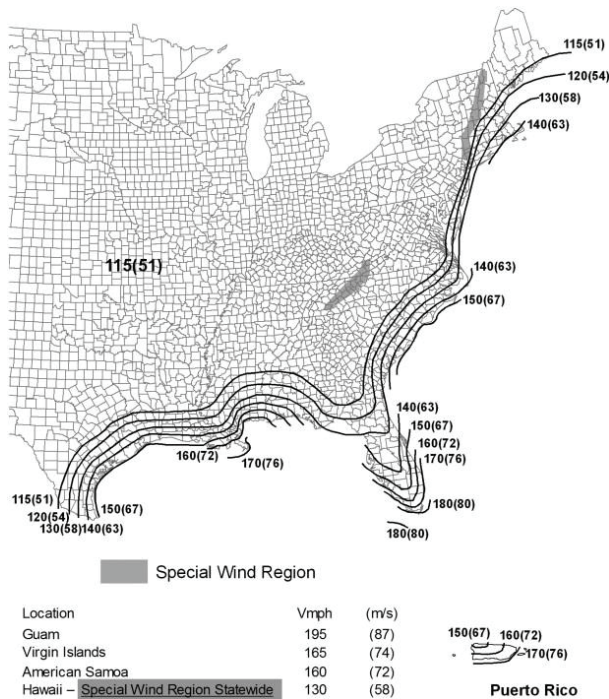


Figure 2 - Wind speeds of workplaces on the east and southeast coasts of the USA

The fragility analysis can be used not only in the field of structural engineering, but also in different areas such as the possibility of trees collapsing at extreme wind speeds. Ciftci et al. [11] explained an approach expected to be used to determine the probability of collapse of trees exposed to windstorm. In their study, this approach was exemplified by using two maple species in the state of Massachusetts, USA. As a result of this study, it has been shown that the applications related to the modeling of the collapse probability of open-grown trees using the probability-based fragility analysis and dynamic time history analysis make a unique contribution to the risk assessment of amenity trees. Lignos and Karamanci [8] discussed the development of the displacement-based and two-parameter fragility curves of steel structural

frames with concentric diagonal members designed for a seismic zone in their study. For steel diagonal elements subjected to periodic loading; drift-based fragility curves have been developed for three damage cases, including local buckling, bending buckling and loss of strength due to rupture of diagonals. The effect of material variety, cross-sectional shape of diagonals and loading protocols on drift-based fragility curves have been investigated. The effects of global and local slenderness ratios on the rupture ductility of steel diagonal elements with different shapes were investigated by using two-parameter fragility curves associated with geometric ratios such as the slenderness ratio together with the expected drift ratios when these previously defined three states occur. Studies have shown that the proposed fragility curves can be used to evaluate quickly the seismic fragility of frames with concentric diagonal members. Shin et al. [12] developed a seismic strengthening scheme with steel struts resistant to buckling for a 2-story steel frame structure designed only for dead loads by using the fragility contour method in their study. Then, using the fragility contour method, the seismic performance of the structure was assessed before and after the strengthening, and the improvement of performance level was evaluated in case of structural collapse or loss of bearing capacity of the structural members. Based on analytical studies, the most effective strut model for the strengthening scheme has been proposed based on various scenarios in terms of the weight of the developed strutting models. This study shows that the fragility contour method can be an effective tool for seismic evaluation and strengthening of structures. Sakurai et al. [13] investigated the contribution of the source of the variables in the moment-rotation characteristics of the connections to the unknowns in the frame deformations by using probability-based finite element analysis to compare the effect of bending stiffness of columns and beams and internal connection stiffness in their study. Probability-based finite element analysis was used to describe the system fragility that defines the probability of exceeding three limit states related to maximum lateral displacement, maximum inter-story drift ratio, and the elastic bending moment capacity which are the function of lateral load. In performance-based design, the effect of variables of internal connection stiffness on frame behavior is very important. The fragility analysis for frame deformation has shown that the coefficient on variation has a significant effect on the performance of frames (especially deformations of frames with complex geometry). Ramirez et al. [14] developed fragility functions that enable to calculate the damages that occur in column-beam connections with welded heads and bolted web built before 1994 in their study. While developing these functions, the experimental results of 51 column-beam connections tested within the scope of 10 different studies conducted in the last 26 years were taken into consideration. When developing the fragility curves, statistical unknowns related to factors based on the development of these curves as a small sample of the experimental results, as well as unknowns due to the difference between samples were taken into account. The results have shown that the developed fragility functions can be easily used by designers and those interested in this work in the performance-based evaluation process to calculate the probability of damage (yielding and crack development) in pre-Northridge column-beam connections which are part of moment-resisting frames after being hit by seismic waves of the considered earthquake scenario. The same functions can be easily used with the probability of exceeding a certain limit to calculate the maximum damage that may occur after the design and the most severe earthquake event considered. Kazantzi et al. [15] determined the arbitrarily chosen unknown system parameters that exist in nature of this structure in order to safely calculate the seismic performance of the 4-story moment-resisting steel frame in this study. Firstly, an advanced numerical model was created by transforming

the strength and plastic deformation properties of this system into three-dimensional parameters. Empirical relationships were derived from the experimental data used to model the periodic behavior of steel sections by using probabilistic distribution parameters including correlation between components. Finally, incremental dynamic analysis and Monte Carlo simulation were used to evaluate completely the seismic performance of the model under the effect of the unknowns. In this study, it was also examined which unknown model parameter would trigger negative demand-capacity correlation in the structural fragility assessment. Considering the structural quality levels (high, moderate and low) in FEMA P-58 and the moment-resisting frame examined, potential demand capacity correlation will likely result in the use of unconventional methods (e.g. fragility analysis) to calculate the fragility of local damage cases (especially where sub-standard quality control is applied during the construction phase) even though there is well agreement with structural demands obtained with or without considering unknown model parameters of very well-designed modern structures. Özel and Güneyisi [16] investigated the seismic reliability of the mid-rise reinforced concrete structures strengthened with eccentric steel braces by using fragility curves. As a result of the studies, four performance limit conditions (slight, moderate, major and collapse) were defined. The fragility curves for these limit states have been developed according to the peak ground acceleration with the log-normal distribution assumption. As a result of this study, improvements in the seismic performance of the mid-rise reinforced concrete structures which are strengthened with different eccentric braces have been achieved by using the formulation of fragility reduction. Kim and Shinozuka [17] examined the results of the fragility curve development for two typical bridge samples in southern California whose columns were reinforced with steel sheathing method against seismic effects in their study. Fragility curves were developed using a two-parameter log-normal distribution as a function of peak ground acceleration. Fragility curves of the bridge before reinforcement and post reinforcement were compared to quantify the improvement in fragility due to reinforcement. The improvement in fragility was determined quantitatively by comparing the median values of the fragility curves plotted before and after reinforcement in order to formulate the problem of developing fragility. The calculated analytical fragility curves corresponding to the damage cases and have an intuitive meaning regarding the design, strengthening and performance of the bridge for earthquake events that occurred in the past. In addition, it was expected that the experimental fragility curves can be much more reliable than the fragility curves derived by other means.

As a result of the literature review, while many studies on seismic fragility analyses of structures have been found, it has been observed that there are fewer studies on wind-induced fragility (e.g., Smith and Caracoglia 2011; Chuang and Spence 2017; Cui and Caracoglia 2019; Ma et al., 2021; Jiang et al., 2023). When these studies are examined, it is noticed that seismic fragility or wind-induced fragility analyses are based fundamentally on the same philosophy and contain great similarities, except for some details in their applications. The wind-induced fragility analysis was also used in this study as a tool to compare and discuss distinct steel structure types under wind loads. In this respect, although this study is not the first to present wind-induced fragility analysis for structures, it is unique in that it expresses and compares the performance-based behavior of two different steel structures (moment resisting and braced frames) under wind loads using fragility analysis. With this concept, in this study, these steel structural frames were designed as symmetrical office buildings having

six spans by considering the previous studies, since the torsion effect are not desired in the structures under consideration [18,19].

Therefore, it was decided to design the structure as an office building [20]. Considering the literature reviews, two different structural frame systems have been selected, namely, moment-resisting frame and braced frame [16, 18, 21–27]. These two frame types were used to provide stability in structures subjected to lateral loads. The fragility curves for these two frame types were plotted by using performance-based analysis method. Firstly, three different performance levels were determined for both frame types, namely, Immediate Occupancy (IO), Life Safety (LS) and Collapse Prevention (CP) using pushover analysis. Then, nonlinear time history analysis method was conducted for the frames depending on the varying wind speeds [28–30]. The number of frames exceeding the displacement limits of the performance levels was determined by comparing the displacement values obtained from the time history analyses with the limit displacement values of the previously determined performance levels. Finally, fragility curves were plotted by considering the number of frames exceeding the limit values of performance levels. According to the results, braced frames can withstand much higher wind speed than moment-resisting frames.

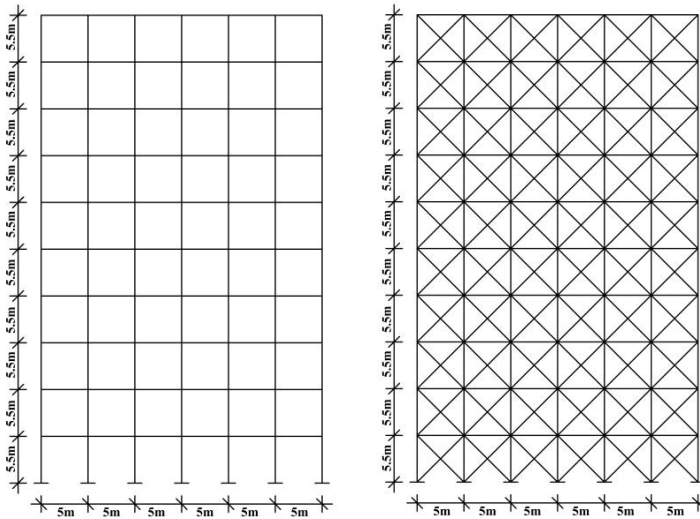


Figure 3 - Considered structural bearing systems a) Frontal view of moment-resisting frame b) Frontal view of braced frame

The focus of this study is to compare the fragility curves of two distinct structure types (the moment resisting frame and the braced frame). In order to apply the fragility analyses to these structural types, it is necessary to select a place corresponding to some assumptions required for all the analyses. The northeastern part of the USA was chosen for the case studies of this research for two reasons. First, this region on earth are often exposed to strong winds. The second reason is to utilize the existing knowledge of the authors, because some of the assumptions used in synthetic wind generation have been used previously for this region.

2. METHODOLOGY

This research contains a case study on the comparison of the fragility curves of two different structural systems (moment-resisting and braced systems) subjected to wind loading. The implementation of these fragility analyses is addressed in the three subtitles of this section that explain the three main steps. As the first step, the cross-sectional areas of the members had already been designed by considering dead loads, live loads, and wind loads. To give more details, the sections for columns, beams, and braces were roughly determined with the preliminary design by considering the live load and wind loads. After the section selections had been made, the load combinations determined according to ASCE 7-10 Section 2.3.2 were defined in the models for each structural system. Then, the design of the sections was finalized using the tool of section checks in the SAP2000 packaged software according to the American Steel Structure Institute Load and Resistance Factor Design (AISC-LRFD). In the second step, the capacity calculations of two structural systems were done using pushover analyses. For these pushover analyses, the needed critical rotations and displacements of the structural members with known cross-sectional areas were found for three performance levels: IO (immediate occupancy), LS (life safety), and CP (collapse prevention). Then, it was revealed that the beams for the moment-resisting system and the braces for the braced system were in charge of controlling all these performance levels, according to the pushover analyses. As the third step, these critical values of the performance levels were used as the limitations of the fragility analyses of the two structural types to be compared with each other.

2.1. A Case Study of Two Structural Systems

In this study, two different structural systems were used, namely the moment-resisting frame and the braced frame (Fig. 3). When a tall building is designed, the time required for analysis can be very long. Therefore, a 10-story steel frame with 5.5 m story height (total height 55 m) was chosen. While making this choice, the Home Insurance Building which is generally regarded as the world's first skyscraper, built in 1885 in Chicago, America and has a 10-story steel frame was taken into consideration [31]. The structural bearing systems used have 6 spans of 5 m length.

Considering the literature on braced frames, in some studies [16,32], diagonal elements were used only in selected bays of the structures, while in others [33–36], they were used in each bay. In this study, as in the examples given above, diagonal members were used in each bay of the braced frame structure. In addition, the column-beam connections used in these braced structures were modeled as pinned joints. Therefore, the lateral force resisting system in braced frames was provided only by the diagonal members used in each bay. In order to have the consistency for the moment resisting frame (MRF) structures with the braced ones, the lateral force resisting system of the MRF structures was provided by the fixed connections at all column-beam joints.

The architecture of the building is designed to be symmetrical as an office building. The spaces in the building (stairwells, elevator shafts etc.) are not taken into account. It was assumed that glass was used as facade material in the building. The weight of this material was ignored. It has been determined that the natural frequencies of the buildings are greater than 1 Hz in both cases, whether they have glass facade or not. For this reason, structures display rigid behavior in these two cases. In this respect, the effect of using facade on the

lateral dynamic behavior of the structures has been neglected, and the structures were modeled using only structural elements.

As it can be seen in Fig.3, considering that the structural system elements and the supports at the base are symmetrical and also that the vertical wind load distribution symmetrically acts on the buildings for each bay, it was decided to analyze these building systems in 2D instead of 3D. In addition, it takes a long time to analyze the structures in three dimensions due to the large number of analyses to be made. Therefore, considering the literature reviews, the structures were modeled and analyzed as two dimensional systems [15]. SAP2000 was used to structural modeling [9,37,38].

As can be seen from Fig. 2, the highest wind speed belongs to Puerto Rico. However, since the wind speed to be applied in the fragility analysis will be above this value, there is no drawback in choosing the city of Boston. The basic wind speed for the city of Boston has been calculated as 62.14 m/s (Fig. 2). Since the structures used are the main wind force resisting systems, wind directionality factor K_d was chosen as 0.85, the exposure category as B, topographic factor K_{zt} as 1.0, wind impact factor G as 0.85, internal pressure coefficient GC_{pi} as +0.18, external pressure coefficient C_p for the windward wall as 0.8, and the C_p for the leeward walls as -0.5, respectively (Table 1).

Table 1 - Parameters used in calculating the wind loads affecting on the frames

K_d	0.85
Exposure Category	B
K_{zt}	1.0
G	0.85
GC_{pi}	0.18

Design wind pressures (see ASCE 7-10 Eq. 27.4-1) and velocity pressures (see ASCE 7-10 Eq. 27.3-1) were separately calculated for windward and leeward directions by using parameters listed in Table 1. For windward direction, the parameter K used in these calculations depends on height. For this reason, the vertical wind profile in windward direction has a non-uniform distribution as shown in Fig. 4. On the other hand, the vertical profile in leeward direction has uniform distribution because the K parameter has a constant value for this direction. In addition, for the calculations of the design wind pressure values in the windward and the leeward directions, the wind speed (V) values come from the wind speed data, which are synthetically generated for each mean speed in the scope of fragility analyses.

After determining the distributed wind load which exerts on buildings, characteristic live loads of the floors were determined according to ASCE 7-10 Table 4-1. Since the buildings to be used in the analysis were designed as office buildings, the characteristic live loads of these structures had been chosen as 2.40 kN/m² [39].

After determining the dead loads, live loads and wind loads for the structures, the building was modeled using Sap2000 [37]. Firstly, the geometrical properties of the structure were

determined. Then, the material properties were obtained. The most commonly used structural steel grades are ASTM A36 and ASTM A992 steels [40]. Structural steel types commonly used in America nowadays are produced according to ASTM A992 standard, which has higher yield and tensile strength than A36 steel [33]. Considering the literature review, the steel grade to be used in the buildings was considered as ASTM A992 [41]. The modulus of elasticity is 200 GPa, Poisson ratio is 0.3, shear modulus is 79.3 GPa, weight per unit volume is 76.9729 kN/m³, mass per unit volume is 7.849 kN/m³, minimum yield stress is 345 MPa and minimum tensile stress is 450 MPa for ASTM A992 steel.

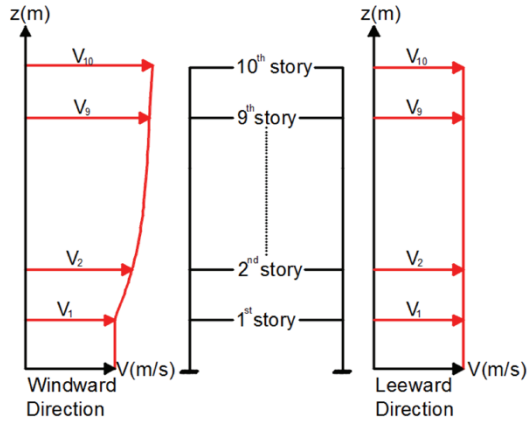


Figure 4 - Wind speed distribution for windward and leeward direction

Then the sections for columns, beams and braces were selected. Since the shear center does not coincide with the center of gravity of the section in singly symmetric double angle and T profiles, torsion effect may occur in these sections. In combined profiles, the compressive strength is affected by the shear transmission strength of the fasteners connecting the elements and the shear resistance of these fasteners [42]. W profile was selected for columns, beams and braces, considering the literature review [8,43]. The section chosen for the columns was W 21x111, for the beams was W 14x53, and for the braces was W 8x67.

After the section selections had been made, three different load models were defined as dead load, live load and wind load.

Nonlinear time history analysis method was used to examine the time-varying effect of loads during the modal analysis. Time history analysis can be conducted by using modal analysis or direct integration method [44]. In this work, eigenvectors were selected. However, modal nonlinear analysis gives better results with Ritz vectors [45]. For this reason, the direct integration method was used for time history analyses.

After the required loads were applied on the structural systems, the load combinations determined according to ASCE 7-10 Section 2.3.2 were defined and the analyses were conducted accordingly these combinations. The load combinations defined are given below [39].

$$1.4D \quad (1)$$

$$1.2D+1.6L+0.5S=1.2D+1.6L(S=0) \quad (2)$$

$$1.2D+1.3W+0.5L+0.5S=1.2D++1.3W+0.5L(S=0) \quad (3)$$

$$0.9D+(1.3W \text{ or } 1.0E)=0.9D+1.3W(E=0) \quad (4)$$

$$0.9D-(1.3W \text{ or } 1.0E)=0.9D-1.3W(E=0) \quad (5)$$

where, dead load is denoted by D, live load by L, snow load by S, earthquake load by E and wind load by W, respectively.

Then, considering the literature reviews, section checks were performed according to the American Steel Structure Institute Load and Resistance Factor Design (AISC-LRFD) method by using the SAP2000 software [46,47].

2.2. Capacity Calculation of Structural Systems

The capacity calculation of the selected structural systems was made by using pushover analysis [28,48, 49]. By applying this method, the structures were subjected to nonlinear static pushover analysis, and the nonlinearity was provided by assigning plastic hinges to the structural elements. The material nonlinear behavior of the elements was modeled by utilizing plastic hinges specified in the FEMA 356 guidelines. According to this regulation, while the plastic hinges of the columns and beams can be determined by moment - rotation relationships, the plastic hinge of the brace members can also be defined using force displacement relationships. The pre-existence of these mechanical relationships in the SAP-2000 program as a default setting provided great convenience for the implementation of this investigation. Since it was possible to obtain the detailed information and values regarding these relationships from the default settings in the SAP-2000 program, it was thought that there is no need to provide them in this text.

In this analysis method, the lateral load model distributed along the height of the structure was used. These lateral loads were then monotonously increased until the structure collapsed or reached the target displacement. Pushover analysis is a simple option to calculate the resistance capacity beyond the elastic region and can be used to determine potential weak zones in the structure [50]. Regarding the lateral load pattern used in pushover analyses, different loading patterns show only a slight change in performance in regular buildings (Abhilash et al. 2009). That is why the equivalent lateral force distribution utilized in FEMA-273 was arbitrarily selected for the pushover analyses addressed in this investigation.

Although two main design criteria are typically considered in ultimate bearing capacity methods (functionality limit, strength limit), there are several design criteria in performance-based design (IO, LS, CP).

It is inevitable for steel structural systems to exhibit nonlinear behavior under load due to the large ductility of steel material. In this regard, pushover analyses are among the most

frequently used techniques in the literature for the performance of these steel structures, as they are a type of nonlinear static analysis [51, 52]. Firstly, plastic hinges for structural members were defined according to ASCE/SEI 41-13 [53] to conduct this analysis. Since columns were mostly affected by axial force and moment, plastic hinges were defined to carry axial force and moment. As beams were mostly affected by moment, plastic hinges were defined to carry moment only. Because braces were only exposed to axial force, the plastic hinges were defined to carry only axial force. Additionally, in this study, the geometric nonlinearity of the pushover and time history analyses was carried out by taking into account P-Delta effects.

The displacement control was performed according to the joint at the top left corner of the frames (Figs. 5(a)-6(a)). As a result of the analysis, pushover curves of the moment-resisting frame and braced frame were obtained (Figs. 5(b)-6(b)). It was concluded that the braced frame started to lose its resistance after 7684.7 kN and the maximum displacement value without occurring collapse for the joint point at the top left corner is 0.085 m from Fig. 5(b). It was also concluded that the moment-resisting frame began to lose its bearing strength after 1651.9 kN and the maximum displacement value without occurring collapse for the joint point at the top left corner was 0.903 m from Fig. 6(b).

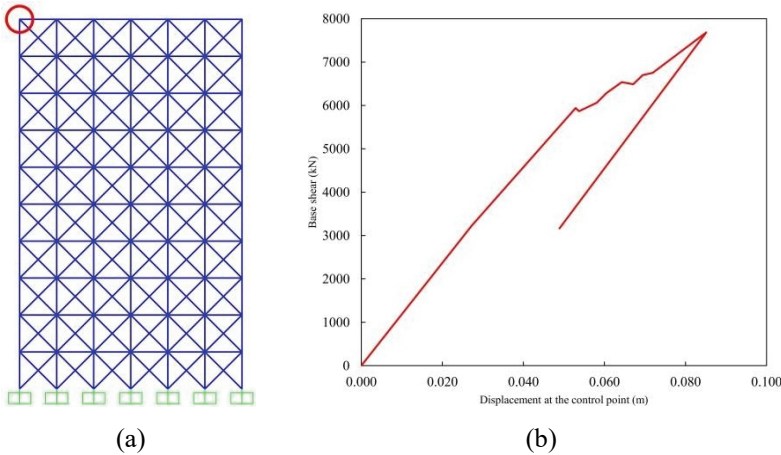


Figure 5 - Pushover analysis results for the braced frame a) The joint where the displacement is checked in the pushover analysis b) The pushover curve of the structure

When Fig. 5(b) and Fig. 6(b) are compared, it is seen that braced frame can carry more load than the moment-resisting frame, while the maximum displacement value of the moment-resisting frame is greater. This shows that although the strength of braced frame is higher, the moment-resisting frame is more ductile.

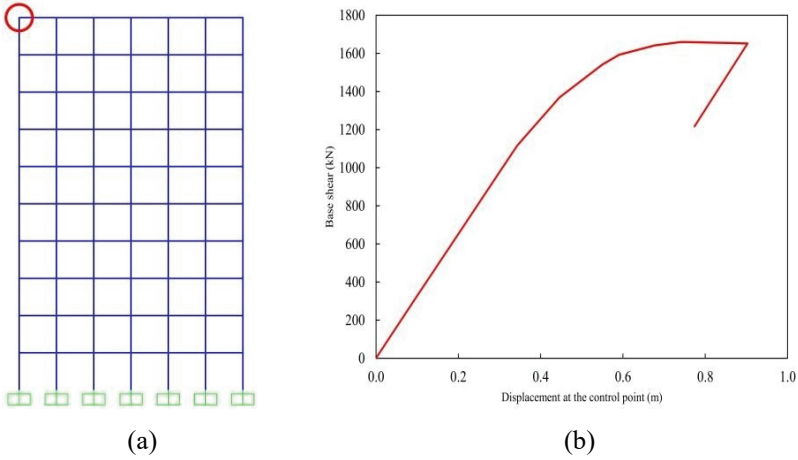


Figure 6 - Pushover analysis results for the moment resisting frame a) The joint where the displacement is checked in the pushover analysis b) The pushover curve of the structure

After the pushover curves of both frames were obtained, structural performance levels were determined on these curves according to ASCE/SEI 41-13 [53]. These levels were divided into three categories as IO, LS and CP Performance levels and were determined by the levels of plastic rotation angles at the beams, and the plastic deformations at the braces according to the standard of ASCE/SEI 41-13 [53]. Acceptance criteria for plastic rotation angles of the beams and plastic deformations of the braces were determined according to equations given in the relevant specification. Table 2 shows these rotation angles and deformations corresponding to the structural members. According to Table 2, the performance levels of IO, LS, and CP occur beyond 0.003, 0.026, and 0.032 in radians respectively, for the beam members. For the brace members, IO, LS, and CP levels start with the plastic deformations having the values 0.002, 0.032, and 0,039 in meters, respectively.

Table 2 - Plastic rotation angles and deformations at the relevant structural members with the performance levels

Performance Levels	Plastic Rotation Angles for Beam Members (rad)	Plastic Deformations for Brace Members (m)
IO	0.003	0.002
LS	0.026	0.032
CP	0.032	0.039

As a result of the performed pushover analysis, it was observed that minor yielding occurred in one beam in the fourth step for the moment-resisting frame. Therefore, the fourth step was determined as the IO performance level. In the fifth step, it was observed that few beams had small-scale yielding but they could still carry shear force. Therefore, the fifth step was determined as the LS performance level. In the sixth step, it was observed that yielding started in one of the columns on the bottom floor of the building and yielding occurred in many beams. Therefore, the sixth step was determined as the CP performance level.

In the braced frame, it was observed that small-scale yielding occurred in one brace in the first step. Therefore, the first step was determined as the IO performance level. In the second step, it was observed that small-scale yielding occurred in few braces, and there was a sudden decrease in the lateral strength of one brace, but it did not lose its strength completely. Therefore, the second step was determined as the LS performance level. In the sixth step, it was observed that there was significant yielding and sudden strength loss in many braces, and small-scale yielding occurred in one of the columns on the bottom floor of the building. Therefore, the sixth step was determined as the CP performance level. In the Table 3, required force and displacements are shown in order for the moment-resisting frame to reach the predetermined performance levels. According to Table 3, in the fourth step of the moment-resisting frame, the displacement of the joint at the upper left corner of the frame was 0.343 m, the corresponding base shear is 1116.6 kN, in the fifth step the displacement of the joint at the top left corner of the frame is 0.446 m, the corresponding base shear is 1368.8 kN, In the sixth step, the displacement of the joint at the top left corner of the frame reached 0.550 m, and the related base shear equaled 1541.9 kN.

Table 3 - Displacement values occurring at the performance levels of the moment-resisting frame

Step	Displacement (m)	Base Shear (kN)
0	0.000	0.0
1	0.100	327.4
2	0.200	651.5
3	0.300	977.1
4	0.343	1116.6
5	0.446	1368.8
6	0.550	1541.9
7	0.591	1592.6
8	0.677	1641.6
9	0.740	1659.7
10	0.755	1659.3
11	0.866	1654.2
12	0.903	1651.9
13	0.774	1216.6

In the Table 4, the required force and displacements are shown in order for the braced frame to reach the predetermined performance levels. According to Table 4, in the first step of the braced frame, the displacement of the joint at the upper left corner of the frame is 0.027 m, the corresponding base shear is 3226.2 kN, in the second step the displacement of the joint at the upper left corner of the frame is 0.053 m, the related base shear is 5941.3 kN, in the sixth step, the displacement of the joint at the top left corner of the frame is 0.064 m and the base shear is 6536.3 kN.

Table 4 - Displacement values occurring at the performance levels of the braced frame

Step	Displacement (m)	Base Shear (kN)
0	0.000	0.0
1	0.027	3226.2
2	0.053	5941.3
3	0.054	5867.0
4	0.058	6061.3
5	0.061	6286.7
6	0.064	6536.3
7	0.067	6489.8
8	0.069	6700.1
9	0.072	6751.4
10	0.085	7684.7
11	0.049	3163.8

2.3. Obtaining Fragility Curves

Fragility functions can be plotted in a single step for the whole structure or in two steps by considering the entire structure and beam-column joints separately [14]. In this study, the fragility curve was created for the entire structure in one step.

In order to plot the fragility curve, firstly, wind models were created depending on the probability. The Ochi-Shin equation was used to determine the wind spectrum for Boston located on the Atlantic ocean coast (Eq. (6)).

$$S_{V_w}(\omega) = \frac{CV_w^2 F_g}{\omega} \tag{6}$$

where, wind spectral density is denoted by $S_{V_w}(\omega)$, surface drag coefficient which is related to surface roughness is denoted by C , mean wind speed (m/s) at 55 m height is denoted by V_w , frequency of wind (rad/s) is denoted by ω and gust factor is denoted by F_g . The Ochi-Shin equation is also very useful in the condition of modifying the surface drag coefficient

which is a physical and singular parameter. Therefore, this equation was chosen while creating the probability based wind model. The C value was modified to use in the considered building systems. F_g value is calculated according to Eq. (7) [11].

$$F_g = \begin{cases} 583((1.592\omega) / V_w) & 0 \leq \omega \leq 0.001885V_w \\ \frac{420((1.592\omega) / V_w)^{0.7}}{(1 + ((1.592\omega) / V_w)^{0.35})^{11.5}} & 0.001885V_w \leq \omega \leq 0.0628V_w \\ \frac{838((1.592\omega) / V_w)}{(1 + ((1.592\omega) / V_w)^{0.35})^{11.5}} & 0.0628V_w \leq \omega \end{cases} \quad (7)$$

The modification process included the calculation of the spectral densities of the changes in wind speed with time in the city of Boston. Then, these spectra were compared with Eq. (6) and defined as in Eq. (9) by changing the C value (Eq. (8)) defined initially [11].

$$C = (750 + 69V_w)(1.0 * 10^{-6}) \quad (8)$$

$$C = (750 + 69V_w)(3.7 * 10^{-6}) \quad (9)$$

Then, the spectral densities of the data obtained from the field were compared with the spectral densities plotted using the modified Ochi-Shin equation. Each of these spectra showed the wind spectrum experimentally generated based on observations of wind records in a very narrow mean wind speed range, and the spectrum plotted by the modified Ochi-Shin equation corresponding to the same average wind speed range. After making these comparisons, wind speed varying with 0.05 s increments in the range of $40 \text{ m/s} \leq V_w \leq 220 \text{ m/s}$ was generated for the reference height (55 m) for finite element model [11].

To produce wind speed data, firstly, for each V_w (wind speed) increase, 100 random wind data were generated by substituting Eq. (9) and Eq. (7) in Eq. (6) and using the spectral method shown in Eq. (10) [11]

$$V_w^G(t) = \sum_{r=1}^n A_r \sin(\omega_r t) + B_r \cos(\omega_r t) \quad (10)$$

Then, the Nataf model was used to transform Gaussian data into time history data series with log-normal marginal distribution which is the most widely used wind speed record distribution type (Eq. (11)).

$$V_i = \frac{\mu x_i^2}{\sqrt{\mu x_i^2 + \sigma x_i^2}} \exp \left(V_i^G \sqrt{\ln \left(\frac{\mu x_i^2 + \sigma x_i^2}{\mu x_i^2} \right)} \right) \quad (11)$$

where, Gaussian variable is denoted by V_i^G , mean is denoted by σx_i^2 and variance is denoted by μx_i . Although the Nataf model distorts the spectrum while transforming it from the

Gaussian space to the non-Gaussian space, this distortion was neglected because it was small (<1%) [11]. One of these time history data is shown in Fig. 7. From this figure, it is seen that wind speeds change in intervals of 0.05 seconds.

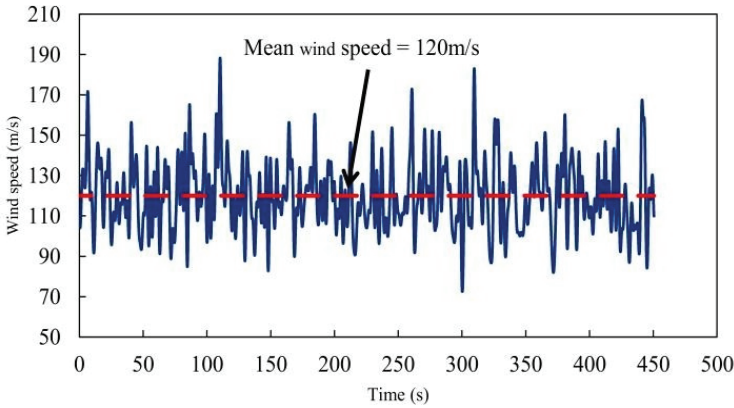


Figure 7 - One of the 100 data generated for an average wind speed of 120 m/s

After generating the wind data, nonlinear time history analyses were conducted on both frames using these data. The mean wind speed values varying between 40-100 m/s were used when conducting time history analyses for moment-resisting frames while the mean wind speed values varying between 70-220 m/s were used when conducting time history analyses for braced frames. Since the time values changed in the range of 0-450.5 seconds in increments of 0.05 seconds, time history analyses were conducted in 9010 steps and 100 analyses were conducted for each mean wind speed. For all these analyses, the damping ratio was used to be 0.02, which is consistent with the literature [54,55].

Then, the number of frames reaching or exceeding predetermined performance levels was calculated and the probability of reaching or exceeding these performance levels for both frames was determined by using these data.

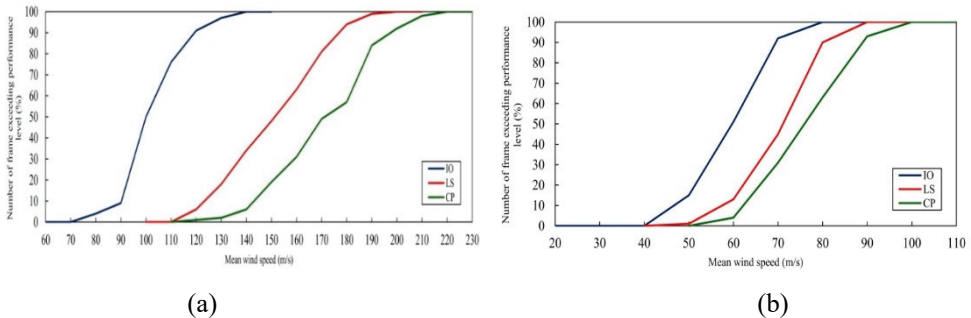


Figure 8 - Number of frames exceeding determined performance level vs mean wind speed
 plot a) Graph for braced frames b) Graph for moment-resisting frames

As a first step to determine these possibilities, graph of mean wind speed vs. number of frames reaching or exceeding the predetermined performance levels for both frame types was plotted using the Monte Carlo (MC) method. For structures with detectable level of failure probability, MC simulation can give precise results to a certain extent [18]. For this reason, in this study, the possibility of reaching or exceeding the predetermined performance levels of the structures was calculated using MC simulation. The number of frames exceeding the predetermined performance level vs. mean wind speed graph obtained by MC method was shown in Fig. 8.

After determining the probability of exceeding the performance levels for the frames depending on the wind speed, the fragility curves for these performance levels were plotted as a last step. When defining the fragility functions, the log-normal cumulative distribution function was generally used (Eq. (12)) [9,10,38,56].

$$P(C | IM = x) = \Phi \left(\frac{\ln(x / \theta)}{\beta} \right) \quad (12)$$

where, possibility of collapse the structure for wind speed corresponding to $IM = x$ is denoted by $P(C | IM = x)$, intensity measure is denoted by IM , standard normal cumulative distribution function is denoted by Φ function, mean of fragility curve (IM level which has 50% possibility of collapse) is denoted by θ and standard deviation of $\ln(IM)$ is denoted by β . In order for Eq. (12) to be adapted to the structure under consideration, the θ and β values obtained from the structural analysis results should be calculated. These parameters were shown as θ and β in calculations [57]. Generally, two different statistical approaches are used to calculate the parameters obtained from the data. The first method is the moments method, which aims to find parameters that show the same sample moment (mean, standard deviation, etc.) distribution of the observation data. The second method is the maximum likelihood estimation (MLE) method, which aims to find the parameters that are distributed in a way to provide the maximum probability of occurrence of the obtained observation data [57].

Since the wind speed used at each intensity measure level varies, the analyst may not fully observe the percentage increase in the collapse probability of the building with the increase in the intensity measure although it is known that the possibility of collapse of the structure will increase with the increase of the intensity measure. The suitable fitting technique for such data is the MLE method used by many researchers [57]. Therefore, the fragility curves were obtained using the MLE method. In this method, the structural analyses generate the number of collapse out of the total number of wind speeds for each $IM = x_j$ intensity measure level. Since the analysis data was obtained at more than one intensity measure level, the likelihood of the whole data set was calculated by the following formula (Eq. (13)).

$$Likelihood = \prod_{j=1}^m \binom{n_j}{z_j} \Phi \left(\frac{\ln(x_j / \theta)}{\beta} \right)^{z_j} \left(1 - \Phi \left(\frac{\ln(x_j / \theta)}{\beta} \right) \right)^{n_j - z_j} \quad (13)$$

where the number of wind speed is denoted by n_j , number of occurring collapses is denoted by z_j and level of intensity measure is denoted by x_j .

In order to calculate the fragility function parameters, the likelihood function in Eq. (13) should be maximized. This operation is equivalent to maximizing the logarithm of the likelihood function (Eq. 14). Thus, it can be easier to find the θ and β parameters.

$$\{\hat{\theta}, \hat{\beta}\} = \arg \max_{\theta, \beta} \sum_{j=1}^m \left\{ \ln \left(\frac{n_j}{z_j} \right) + z_j \ln \Phi \left(\frac{\ln(x_j / \theta)}{\beta} \right) + (n_j - z_j) \ln \left(1 - \ln \Phi \left(\frac{\ln(x_j / \theta)}{\beta} \right) \right) \right\} \quad (14)$$

Fragility curves were plotted in computer environment for three different performance levels (IO, LS, CP) of moment-resisting frames and braced frames, depending on the MC data.

3. RESULTS AND DISCUSSIONS

As mentioned before, this research was conducted as a case study focusing on the comparison of the fragility analyses of two distinct structure types (moment-resisting and braced frames). Therefore, the results obtained with this research belong to the two different structural systems discussed within the case study, and these results are only recommended for other structural systems but not inclusive of all. Additionally, to repeat, it can be stated that this study focused on comparing the fragility curves of two different structural systems (moment-resisting and braced frames). For this comparison, all the mechanical properties of the beams in each system, such as the amount and cross-sectional areas (W14x53), were assigned the same. This situation was also true for columns (W21x111). Both structural systems offer only one different feature among themselves. This difference is that, while there are no cross members in the moment-resisting frame system, which can carry moments at the joints, the braced frame system has those cross members that carry axial loads. These structural frame systems have been analyzed as 2D for this study. Therefore, the differences between the fragility curves of these structural systems, which are equivalent in terms of all their features but differ in only one aspect, have explored and revealed more consistently and accurately.

The data obtained by MC and MLE method are shown in Fig. 9. In this figure, red line shows the results obtained from the calculations made according to the MLE method, while the blue points show the results obtained from the calculations made according to the MC method.

According to Fig. 9(a), no frame exceeds the IO performance level for 40 m/s average wind speed in moment-resisting frames. In addition, it is also seen that all frames exceed IO performance level for 80 m/s when MC method is used in calculations and for 100 m/s when MLE is used in calculations.

According to Fig. 9(b), no frame exceeds LS performance level for 40 m/s average wind speed in moment-resisting frames. In addition, it is also seen that all frames exceed LS performance level for 90 m/s when MC method is used in calculations and for 100 m/s when MLE is used in calculations.

According to Fig. 9(c), no frame exceeds CP performance level for 40 m/s average wind speed in moment-resisting frames. In addition, it is also seen that all frames exceed CP performance level for 100 m/s when MC or MLE method is used in calculations.

According to Fig. 9(d), no frame exceeds IO performance level for 70 m/s average wind speed in braced frames. In addition, it is also seen that all frames exceed IO performance

level for 140 m/s when MC method is used in calculations and for 150 m/s when MLE is used in calculations.

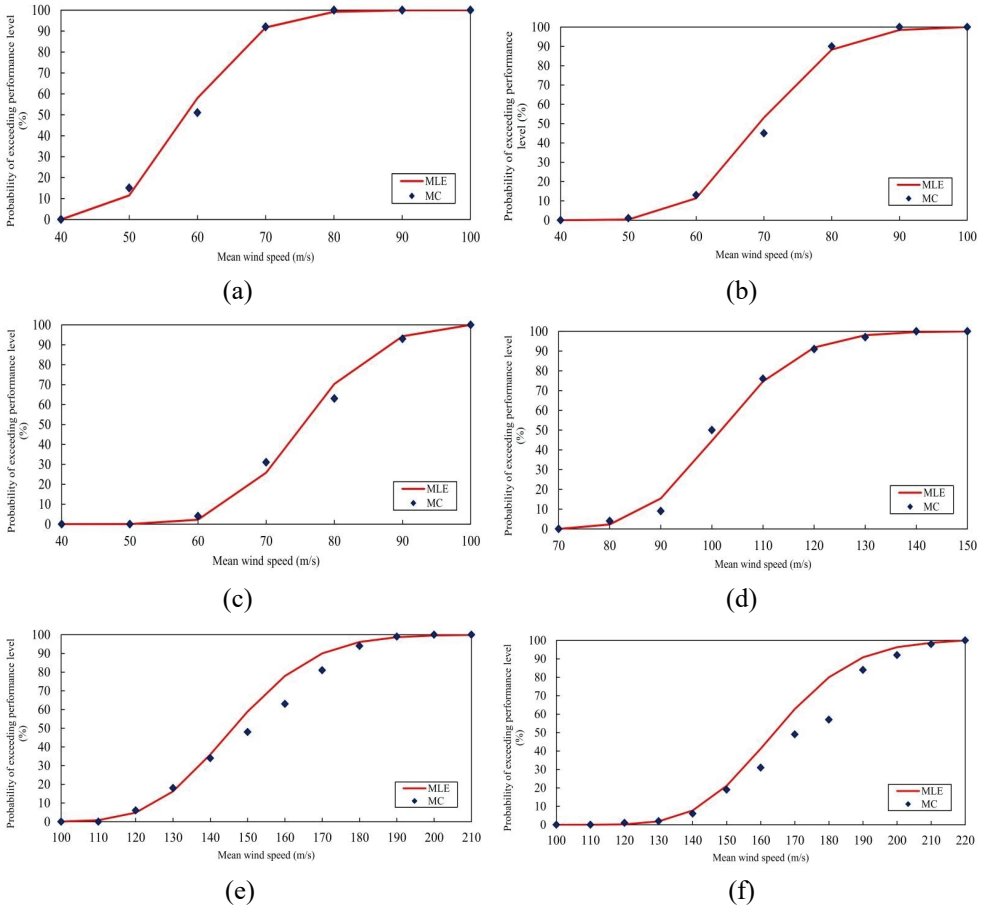


Figure 9 - Plots for probabilities of exceeding predetermined performance levels depending on changing wind speeds for frames a) Probability of exceeding IO performance level for moment-resisting frames b) Probability of exceeding LS performance level for moment-resisting frames c) Probability of exceeding CP performance level for moment-resisting frames d) Probability of exceeding IO performance level for braced frames e) Probability of exceeding LS performance level for braced frames f) Probability of exceeding CP performance level for braced frames

According to Fig. 9(e), no frame exceeds LS performance level for 100 m/s average wind speed in braced frames. In addition, it is also seen that all frames exceed LS performance level for 200 m/s when MC method is used in calculations and for 210 m/s when MLE is used in calculations.

According to Fig. 9(f), no frame exceeds CP performance level for 110 m/s average wind speed in braced frames. In addition, it is also seen that all frames exceed CP performance level for 220 m/s when MC or MLE method is used in calculations.

In addition, yielding starts and then collapse occurs in the mean wind speed range of 40-100 m/s in the moment-resisting frame, while yielding starts and then collapse occurs in the wind speed range of 70-220 m/s in the braced frame. Considering that hurricanes have a variable wind speed range, it can be stated that it is more advantageous if the process between yielding and collapse of structures takes place in a wider wind range.

Table 5 - Comparison of performances of the moment-resisting frame and braced frame under varying mean wind speeds

Mean wind speed (m/s)	Number of Analyses	Probability of exceeding performance level according to MLE method (%)					
		Braced frame			Moment-resisting frame		
		IO	LS	CP	IO	LS	CP
40	100	0.00	0.00	0.00	0.00	0.00	0.00
50	100	0.00	0.00	0.00	11.51	0.32	0.01
70	100	0.00	0.00	0.00	91.75	53.10	25.86
80	100	2.25	0.83	0.02	99.21	88.31	70.37
100	100	44.62	0.00	0.00	100.00	100.00	100.00
150	100	100.00	58.89	21.18	100.00	100.00	100.00
210	100	100.00	100.00	98.72	100.00	100.00	100.00
220	100	100.00	100.00	100.00	100.00	100.00	100.00

Table 6 - Quantity calculation for moment-resisting frame

Steel section type	Number of steel section used	Cross sectional area (m ²)	Total length (m)	Density (kg/m ³)	Total weight of steel used (kg)	Total weight of structure (kg)
W14*53	60	0.010064	300	7849.1	23698	87451
W21*111	70	0.021097	385	7849.1	63753	
W14*53	60	0.010064	300	7849.1	23698	
W21*111	70	0.021097	385	7849.1	63753	

Table 7 - Quantity calculation for braced frame

Steel section type	Number of steel section used	Cross sectional area (m ²)	Total length (m)	Density (kg/m ³)	Total weight of steel section used(kg)	Total weight of structure (kg)
W14*53	60	0.010064	300	7849.1	23698	176439
W21*111	70	0.021097	385	7849.1	63753	
W8*67	120	0.01271	892	7849.1	88988	
W14*53	60	0.010064	300	7849.1	23698	

Performances of moment-resisting frame and braced frame under varying mean wind speeds are compared in Table 5. According to this table, moment-resisting frame exceeds the performance levels IO, LS and CP with 100% probability for 100 m/s mean wind speed. Braced frame exceeds the IO performance level with 100% probability for 150 m/s mean wind speed, LS performance level with 100% probability for 210 m/s mean wind speed, and CP performance level with 100% probability for 220 m/s mean wind speed. In addition, the performance level IO, LS and CP for the moment-resisting frame is exceeded at the same mean wind speed. This indicates that the moment resisting frame, which is addressed in this study, performs more brittle behavior than the other structure. Finally, quantities of both frame types were calculated in order to form an opinion in terms of cost-performance. As a result of the quantity calculations, the total weight of the moment-resisting frame was found to be 87451 kg, and the total weight of the braced frame was found to be 176439 kg (Tables 6-7).

The sample size-a crucial boundary condition parameter for Monte Carlo simulations-has a significant effect on having smoother fragility curves calculated in the article. In this context, increasing the sample size used in each fragility curve calculation would have made the results more stable. However, in spite of this benefit, a serious drawback would have also come to light. This drawback was that increasing the sample size would significantly increase both the workload and the amount of time required for the fragility analyses [58]. However, as can be understood from the title of this study, this article is actually about the comparison of the performances of different structure types under wind load, and the fragility curves have been used as only a tool for these comparisons. In this regard, the authors think that the sample size used for these comparisons is sufficient for its objective. As a matter of fact, the literature also contains several studies with smaller sample sizes than the sample size utilized in this study.

4. CONCLUSIONS

In this study, the efficiency of of braces was investigated by comparing the fragility curves of moment-resisting and braced frames under wind loads. As a result of these comparisons, it has been seen that using diagonal members is of great importance in terms of improving structural performance. At the different performance levels (IO, LS, CP), the fragility curves of the braced frame have a broader distribution feature than those of the moment resisting frame in respect to the mean wind speed values.

In addition to all these, yielding starts and then collapse occurs in the mean wind speed range of 40-100 m/s in the moment-resisting frame, while yielding starts and then collapse occurs in the wind speed range of 70-220 m/s in the braced frame. Considering that hurricanes have a variable wind speed range, it can be stated that it is more advantageous if the process between yielding and collapse of structures takes place in a higher wind range.

When the total weight of the two frame types used is compared, it is seen that braced frames are two times heavier than moment-resisting frames (Tables 6-7). However, the mean wind speed required to cause heavy damage to the structural members (LS performance level) with 100% probability for the braced frame is more than twice that for the moment-resisting frame. Similarly, the mean wind speed needed to cause collapse to the structural members (CP performance level) with 100% certainty is over twice as high for the braced frame

compared to the moment-resisting frame. While infrequent, these severe wind speeds have the potential to result in significant loss of life and property. Thus, it is important to consider these average wind speeds while designing buildings in hurricane-prone areas.

Symbols

K_d wind directionality factor

K_{zt} topographic factor

G impact factor

GC_{pi} internal pressure coefficient

V wind speed

D dead load

L live load

S snow load

E earthquake load

$S_{V_w}(\omega)$ wind spectral density

C surface roughness coefficient

V_w mean wind speed at specific height

F_g gust factor

V_i^G Gaussian variable

σx_i mean

μx_i variance

$P(C | IM = x)$ is the possibility of collapse the structure for wind speed corresponding to $IM = x$

IM intensity measure

θ mean fragility curve

β standard deviation of $\ln(IM)$

z_j number of occurring collapses

n_j is the number of wind speed

x_j is the level of intensity measure

Acknowledgements

This research did not receive any specific grant from funding agencies in the public, commercial, or not-for-profit sectors.

References

- [1] 3TIER, Global Mean Wind Speed at 80 m, University of Utah (2011). https://www.inscc.utah.edu/~krueger/5270/3tier_5km_global_wind_speed.pdf (accessed September 25, 2022).
- [2] American Society of Civil Engineers, ASCE/SEI 7-10: Minimum design loads for buildings and other structures, 3rd ed., American Society of Civil Engineers, Virginia, 2013.
- [3] W. Cui, L. Caracoglia, Exploring hurricane wind speed along US Atlantic coast in warming climate and effects on predictions of structural damage and intervention costs, *Eng Struct* 122 (2016) 209–225. <https://doi.org/10.1016/J.ENGSTRUCT.2016.05.003>.
- [4] R.K. Tessari, H.M. Kroetz, A.T. Beck, Performance-based design of steel towers subject to wind action, *Eng Struct* 143 (2017) 549–557. <https://doi.org/10.1016/J.ENGSTRUCT.2017.03.053>.
- [5] Y.J. Cha, J.W. Bai, Seismic fragility estimates of a moment-resisting frame building controlled by MR dampers using performance-based design, *Eng Struct* 116 (2016) 192–202. <https://doi.org/10.1016/J.ENGSTRUCT.2016.02.055>.
- [6] M. Ansari, A. Safiey, M. Abbasi, Fragility based performance evaluation of mid rise reinforced concrete frames in near field and far field earthquakes, *Structural Engineering and Mechanics* 76 (2020) 751. <https://doi.org/10.12989/SCS.2020.76.6.751>.
- [7] P. Liu, Z.-H. Li, W.-G. Yang, Seismic fragility analysis of sliding artifacts in nonlinear artifact-showcase-museum systems, *Structural Engineering and Mechanics* 78 (2021) 333. <https://doi.org/10.12989/SEM.2021.78.3.333>.
- [8] D.G. Lignos, E. Karamanci, Drift-based and dual-parameter fragility curves for concentrically braced frames in seismic regions, *J Constr Steel Res* 90 (2013) 209–220. <https://doi.org/10.1016/J.JCSR.2013.07.034>.
- [9] A. Gürbüz, M. Tekin, Farklı Tip Betonarme Binalar İçin Geliştirilmiş Hasar Tahmin Yöntemleri, *Teknik Dergi* 28 (2017) 8051–8076. <https://doi.org/10.18400/TEKDERG.334196>.
- [10] M. Salameh, M. Shayanfar, M.A. Barkhordari, Seismic Performance of a Hybrid Coupled Wall System Using different Coupling Beam Arrangements, *Teknik Dergi* 33 (2022) 12401–12428. <https://doi.org/10.18400/TEKDERG.782642>.
- [11] C. Ciftci, S.R. Arwade, B. Kane, S.F. Brena, Analysis of the probability of failure for open-grown trees during wind storms, *Probabilistic Engineering Mechanics* 37 (2014) 41–50. <https://doi.org/10.1016/J.PROBENGMECH.2014.04.002>.
- [12] J. Shin, K. Lee, S.H. Jeong, J. Lee, Probabilistic performance assessment of gravity-designed steel frame buildings using buckling-restrained knee braces, *J Constr Steel Res* 104 (2015) 250–260. <https://doi.org/10.1016/J.JCSR.2014.10.019>.

- [13] S. Sakurai, B.R. Ellingwood, S. Koshiyama, Probabilistic study of the behavior of steel frames with partially restrained connections, *Eng Struct* 23 (2001) 1410–1417. [https://doi.org/10.1016/S0141-0296\(01\)00052-9](https://doi.org/10.1016/S0141-0296(01)00052-9).
- [14] C.M. Ramirez, D.G. Lignos, E. Miranda, D. Kolios, Fragility functions for pre-Northridge welded steel moment-resisting beam-to-column connections, *Eng Struct* 45 (2012) 574–584. <https://doi.org/10.1016/J.ENGSTRUCT.2012.07.007>.
- [15] A.K. Kazantzi, D. Vamvatsikos, D.G. Lignos, Seismic performance of a steel moment-resisting frame subject to strength and ductility uncertainty, *Eng Struct* 78 (2014) 69–77. <https://doi.org/10.1016/J.ENGSTRUCT.2014.06.044>.
- [16] A.E. Özel, E.M. Güneysi, Effects of eccentric steel bracing systems on seismic fragility curves of mid-rise R/C buildings: A case study, *Structural Safety* 33 (2011) 82–95. <https://doi.org/10.1016/J.STRUSAFE.2010.09.001>.
- [17] S.H. Kim, M. Shinozuka, Development of fragility curves of bridges retrofitted by column jacketing, *Probabilistic Engineering Mechanics* 19 (2004) 105–112. <https://doi.org/10.1016/J.PROBENGMECH.2003.11.009>.
- [18] S. Bobby, S.M.J. Spence, E. Bernardini, A. Kareem, Performance-based topology optimization for wind-excited tall buildings: A framework, *Eng Struct* 74 (2014) 242–255. <https://doi.org/10.1016/J.ENGSTRUCT.2014.05.043>.
- [19] F. Mazza, M. Fiore, Vibration control by damped braces of fire-damaged steel structures subjected to wind and seismic loads, *Soil Dynamics and Earthquake Engineering* 83 (2016) 53–58. <https://doi.org/10.1016/J.SOILDYN.2016.01.003>.
- [20] Y. Gong, Y. Xue, L. Xu, Optimal capacity design of eccentrically braced steel frameworks using nonlinear response history analysis, *Eng Struct* 48 (2013) 28–36. <https://doi.org/10.1016/J.ENGSTRUCT.2012.10.001>.
- [21] A. Arablouei, V. Kodur, A fracture mechanics-based approach for quantifying delamination of spray-applied fire-resistive insulation from steel moment-resisting frame subjected to seismic loading, *Eng Fract Mech* 121–122 (2014) 67–86. <https://doi.org/10.1016/J.ENGFRACMECH.2014.03.003>.
- [22] A. Imanpour, K. Auger, R. Tremblay, Seismic design and performance of multi-tiered steel braced frames including the contribution from gravity columns under in-plane seismic demand, *Advances in Engineering Software* 101 (2016) 106–122. <https://doi.org/10.1016/J.ADVENGSOFT.2016.01.021>.
- [23] J. Iyama, H. Kuwamura, Probabilistic advantage of vibrational redundancy in earthquake-resistant steel frames, *J Constr Steel Res* 52 (1999) 33–46. [https://doi.org/10.1016/S0143-974X\(99\)00012-7](https://doi.org/10.1016/S0143-974X(99)00012-7).
- [24] Y.C. Lin, Steel sliding-controlled coupled beam modules: Development and seismic behavior for a moment resisting frame, *Eng Struct* 99 (2015) 726–736. <https://doi.org/10.1016/J.ENGSTRUCT.2015.05.008>.
- [25] D.B. Merczel, J.M. Aribert, H. Somja, M. Hjiiaj, Plastic analysis-based seismic design method to control the weak storey behaviour of concentrically braced steel frames, *J Constr Steel Res* 125 (2016) 142–163. <https://doi.org/10.1016/J.JCSR.2016.05.008>.

- [26] M. Pirizadeh, H. Shakib, Probabilistic seismic performance evaluation of non-geometric vertically irregular steel buildings, *J Constr Steel Res* 82 (2013) 88–98. <https://doi.org/10.1016/J.JCSR.2012.12.012>.
- [27] P. Sultana, M.A. Youssef, Seismic performance of steel moment resisting frames utilizing superelastic shape memory alloys, *J Constr Steel Res* 125 (2016) 239–251. <https://doi.org/10.1016/J.JCSR.2016.06.019>.
- [28] J. Alam, D. Kim, B. Choi, Seismic risk assessment of intake tower in Korea using updated fragility by Bayesian inference, *Structural Engineering and Mechanics* 69 (2019) 317. <https://doi.org/10.12989/SEM.2019.69.3.317>.
- [29] JavadMoradloo, K. Naserasadi, H. Zamani, Seismic fragility evaluation of arch concrete dams through nonlinear incremental analysis using smeared crack model, *Structural Engineering and Mechanics* 68 (2018) 747. <https://doi.org/10.12989/SEM.2018.68.6.747>.
- [30] P. Liu, H.X. Zhu, P.P. Fan, W.G. Yang, A reliability-based fragility assessment method for seismic pounding between nonlinear buildings, *Structural Engineering and Mechanics* 77 (2021) 19–35. <https://doi.org/10.12989/SEM.2021.77.1.019>.
- [31] G. Craighead, *High-Rise Security and Fire Life Safety*, 3rd ed., Butterworth-Heinemann, Boston, 2009.
- [32] J.-W. Lai, S.A. Mahin, Strongback System: A Way to Reduce Damage Concentration in Steel-Braced Frames, *Journal of Structural Engineering* 141 (2014) 04014223. [https://doi.org/10.1061/\(ASCE\)ST.1943-541X.0001198](https://doi.org/10.1061/(ASCE)ST.1943-541X.0001198).
- [33] T. Okazaki, M.D. Engelhardt, Cyclic loading behavior of EBF links constructed of ASTM A992 steel, *J Constr Steel Res* 63 (2007) 751–765. <https://doi.org/10.1016/J.JCSR.2006.08.004>.
- [34] S. Kazemzadeh Azad, C. Topkaya, A review of research on steel eccentrically braced frames, *J Constr Steel Res* 128 (2017) 53–73. <https://doi.org/10.1016/J.JCSR.2016.07.032>.
- [35] D.M. Patil, K.K. Sangle, Seismic Behaviour of Different Bracing Systems in High Rise 2-D Steel Buildings, *Structures* 3 (2015) 282–305. <https://doi.org/10.1016/J.ISTRUC.2015.06.004>.
- [36] R. Sabelli, S. Mahin, C. Chang, Seismic demands on steel braced frame buildings with buckling-restrained braces, *Eng Struct* 25 (2003) 655–666. [https://doi.org/10.1016/S0141-0296\(02\)00175-X](https://doi.org/10.1016/S0141-0296(02)00175-X).
- [37] Computers and Structures Inc., Sap2000 v19.0.0, (2016).
- [38] T. Uçar, M. Düzgün, Betonarme Binalar İçin Artımsal İtme Analizi Esaslı Analitik Hasargörebilirlik Eğrilerinin Oluşturulması, *Teknik Dergi* 24 (2013) 402. <https://dergipark.org.tr/tr/pub/tekderg/issue/12741/155127> (accessed July 18, 2024).
- [39] American Society of Civil Engineers, *ASCE/SEI 7-10: Minimum design loads for buildings and other structures*, 3rd ed., American Society of Civil Engineers, Virginia, 2013.

- [40] R. Bjorhovde, The 2005 American steel structures design code, *J Constr Steel Res* 62 (2006) 1068–1076. <https://doi.org/10.1016/J.JCSR.2006.06.011>.
- [41] M. Haddad, Cyclic behavior and finite element modeling of wide flange steel bracing members, *Thin-Walled Structures* 111 (2017) 65–79. <https://doi.org/10.1016/J.TWS.2016.11.006>.
- [42] C.G. Salmon, J.E. Johnson, F.A. Malhas, *Steel Structures Design and Behavior*, 5th ed., Prentice Hall, New Jersey, 2008.
- [43] J. Szalai, F. Papp, On the probabilistic evaluation of the stability resistance of steel columns and beams, *J Constr Steel Res* 65 (2009) 569–577. <https://doi.org/10.1016/J.JCSR.2008.08.006>.
- [44] CSi Knowledge Base, Time-History Analysis, Computers and Structures Inc. (2014). <https://wiki.csiamerica.com/display/kb/Time-history+analysis> (accessed September 25, 2022).
- [45] CSi Knowledge Base, Ritz vs. Eigen Vectors, Computers and Structures Inc. (2014). <http://wiki.csiamerica.com/display/kb/Ritz+vs.+Eigen+vectors> (accessed September 25, 2022).
- [46] American Institute of Steel Construction, *Manual of Steel Construction: Load and Resistance Factor Design*, 3rd ed., American Institute of Steel Construction, Illinois, 2001.
- [47] American Institute of Steel Construction, *Steel Construction Manual*, 15th ed., American Institute of Steel Construction, Illinois, 2017.
- [48] L.-X. Li, H.-N. Li, C. Li, Seismic fragility assessment of self-centering RC frame structures considering maximum and residual deformations, *Structural Engineering and Mechanics* 68 (2018) 677. <https://doi.org/10.12989/SEM.2018.68.6.677>.
- [49] Y. Lu, L. Zhang, Z. He, F. Feng, F. Pan, Wind-induced vibration fragility of outer-attached tower crane to super-tall buildings: A case study, *Wind and Structures* 32 (2021) 405. <https://doi.org/10.12989/WAS.2021.32.5.405>.
- [50] S. Li, Z. Zuo, C. Zhai, L. Xie, Comparison of static pushover and dynamic analyses using RC building shaking table experiment, *Eng Struct* 136 (2017) 430–440. <https://doi.org/10.1016/J.ENGSTRUCT.2017.01.033>.
- [51] M. Bocciarelli, G. Barbieri, A numerical procedure for the pushover analysis of masonry towers, *Soil Dynamics and Earthquake Engineering* 93 (2017) 162–171. <https://doi.org/10.1016/J.SOILDYN.2016.07.022>.
- [52] K. Kamath, S. Hirannaiah, J.C.K.B. Noronha, An analytical study on performance of a diagrid structure using nonlinear static pushover analysis, *Perspect Sci (Neth)* 8 (2016) 90–92. <https://doi.org/10.1016/J.PISC.2016.04.004>.
- [53] American Society of Civil Engineers, *ASCE/SEI 41-13: Seismic Evaluation and Retrofit of Existing Buildings*, 1st ed., American Society of Civil Engineers, Virginia, 2014.

- [54] F.N. Kudu, Ş. Uçak, G. Osmancikli, T. Türker, A. Bayraktar, Estimation of damping ratios of steel structures by Operational Modal Analysis method, *J Constr Steel Res* 112 (2015) 61–68. <https://doi.org/10.1016/J.JCSR.2015.04.019>.
- [55] A. V. Papageorgiou, C.J. Gantes, Equivalent modal damping ratios for concrete/steel mixed structures, *Comput Struct* 88 (2010) 1124–1136. <https://doi.org/10.1016/J.COMPSTRUC.2010.06.014>.
- [56] M.S. Kırçıl, E.Ç. Kocabey, Examination of the Efficiency of Retrofitting Methods through Fragility Analysis, *Teknik Dergi* 30 (2019) 9243–9260. <https://doi.org/10.18400/TEKDERG.408126>.
- [57] Baker Research Group, Efficient Analytical Fragility Function Fitting Using Dynamic Structural Analysis, Stanford University (2014). <http://web.stanford.edu/~bakerjw/publications.html> (accessed September 25, 2022).
- [58] C. Çiftçi, A Methodology for Fast and Accurate Analytical Fragility Analysis of Linear Structural Systems during Wind Storms: ALFA, *Erciyes Üniversitesi Fen Bilimleri Enstitüsü Fen Bilimleri Dergisi* 39 (2023) 508-520.

